



Pb(II) and Zn(II) adsorption onto Na- and Ca-montmorillonites in acetic acid/acetate medium:
Experimental approach and geochemical modelling

Authors

Mariem GHAYAZA¹, Lydie LE FORESTIER^{1,2*}, Fabrice MULLER¹, Christophe
TOURNASSAT³, Jean-Michel BENY¹

Address

¹Université d'Orléans, Université François Rabelais – Tours, CNRS/INSU, Institut des
Sciences de la Terre d'Orléans - UMR 6113, Campus Géosciences, 1A rue de la Férollerie,
45071 Orléans cedex 2, France

²Université d'Orléans, Université François Rabelais – Tours, CNRS/INSU, Institut des
Sciences de la Terre d'Orléans - UMR 6113, Polytech'Orléans, 8 rue Léonard de Vinci, 45072
Orléans cedex 2, France

³BRGM, 3 avenue Claude Guillemin, 45060 Orléans Cedex 2, France

**Corresponding author:*

E-mail address: lydie.leforestier@univ-orleans.fr

Telephone number: +33 2 38 25 53 93

Fax number: +33 2 38 63 64 88

Abstract

Smectites are usually used as a clay barrier at the bottom of subsurface waste landfills due to their low permeability and their capacity to retain pollutants. The Na- and Ca-saturated SWy2 montmorillonites were interacted with initial $\text{Zn}(\text{NO}_3)_2$ or $\text{Pb}(\text{NO}_3)_2$ concentrations ranging from 10^{-6} to 10^{-2} M with a solid/liquid ratio of 10 g L^{-1} , and using acetic acid/acetate as buffer at pH 5 in order to reproduce a biodegradable leachate of a young landfill. These experiments revealed that Zn and Pb sorption onto Na-SWy2 is higher than onto Ca-SWy2 in the whole range of concentrations. Metal retention into both montmorillonites increases with the decrease in acetic acid/acetate concentration. The two site protolysis model with no electrostatic term (2SPNE model) was used to model these experiments. As the experimental data of Zn sorption were well fitted, this model was validated and has been improved by taking into account the metal-acetate complexation in solution. In order to validate the model for Pb sorption, new selectivity coefficients have been determined, namely $\log K_c(\text{Pb-Na}) = 0.5$ for Na-montmorillonite and $\log K_c(\text{Pb-Ca}) = 0.3$ for Ca-montmorillonite.

Key words: adsorption; lead; zinc; cation exchange; surface complexation

1. Introduction

The major potential environmental impacts related to landfill leachate are pollution of groundwater and surface water. European legislation requires the presence of a clay barrier at the bottom of waste landfills to prevent contamination. Smectites are usually used for this purpose because of their low permeability, their expansion ability and their capacity to retain pollutants. When refuse is buried in a landfill, a complex series of biological and chemical reactions occur as the refuse decomposes. It is generally accepted that landfills undergo five phases of decomposition: (1) an initial aerobic phase, which lasts only a few days, (2) an anaerobic acid phase, (3) an initial methanogenic phase, (4) a stable methanogenic phase, and (5) an additional aerobic or humic phase of decomposition [1]. Leachate composition mainly depends on the biodegradation phase of the organic matter, and hence on the age of the waste disposal. Consequently, three types of leachate have been distinguished [2]: biodegradable for a young landfill (< 5 years old), intermediate for a medium landfill (5-10 years), and stabilized for an old landfill (> 10 years). The biodegradable leachate is characterized by a decrease in pH ($4.5 < \text{pH} < 6.5$), due to the accumulation of volatile fatty acids, principally carboxylic acids, resulting from bacterial activity. Harmsen [3] estimated that 95% of the total organic carbon comes from these acids. As the pH is acidic, this leachate is chemically aggressive and will increase the solubility of many compounds, in particular of heavy metals (up to 2 g L^{-1}). The organic acids are then progressively converted to methane and carbon dioxide by methanogenic bacteria, leading to an increase in pH. Thus, the intermediate leachate is characterized by a neutral environment ($6.5 < \text{pH} < 7.5$) and a low biodegradability due to a lower content of volatile fatty acids. Finally, the stabilized leachate contains fulvic and humic acids of a high molecular weight, and also low molecular weight compounds, all of which are resistant to biodegradation. The leachate produced by an old landfill is basic with a pH between 7.5 and 9. Consequently, the major potential pollution of surface water and

groundwater may be caused by the acidic leachates of young landfills containing high amounts of toxic metals. Two of the most abundant metallic pollutants present in waste landfill leachates are lead and zinc. Pb occurs predominantly as Pb^{2+} species up to pH 6, with also the presence of a nitrate species $PbNO_3^+$ (less than 10%) [4], whereas all zinc is in the form of Zn^{2+} at pH 5. Zinc is known to be essential to plants, humans and animals, but it can have adverse effects if its availability in soils exceeds a certain threshold value. Acute toxicity arises from the ingestion of excessive amounts of zinc salts, either accidentally or deliberately after the consumption of more than 500 mg of zinc sulfate. Lead is known to be hazardous even at low concentrations. To avoid the contamination of the water table and consequently the contamination of living beings, it is essential to predict the behaviour of these metals in the clay barrier of waste landfills. The mean landfill concentration values are 5 mg L^{-1} ($7.6 \times 10^{-5} \text{ mol L}^{-1}$) for zinc and 0.09 mg L^{-1} ($4.3 \times 10^{-7} \text{ mol L}^{-1}$) for lead [5]. The maximum reported concentrations can however reach 1000 mg L^{-1} ($1.5 \times 10^{-2} \text{ mol L}^{-1}$) for zinc and 5 mg L^{-1} ($2.4 \times 10^{-5} \text{ mol L}^{-1}$) for lead. All these values exceed international standards for drinking water, which are 3 mg L^{-1} ($= 4.6 \times 10^{-5} \text{ mol L}^{-1}$) for Zn and 0.01 mg L^{-1} ($= 4.8 \times 10^{-8} \text{ mol L}^{-1}$) for Pb [6].

Numerous experimental studies have investigated the interaction between clays and lead or zinc, where factors such as pH [7,8], ionic strength [9,10], or clay adsorbents such as kaolinite, illite or montmorillonite [4,8,11,12] affect the extent of adsorption of these metals onto clays. However, these metallic pollutants are in contact with other compounds in leachates (dissolved organic matter, inorganic macro components, and xenobiotic organic compounds), which may influence the interactions of metals with clay. Gautier et al. [13] have shown that carboxylic acids may interact with smectite, while Huang et al. [14] have studied the influence of low molar mass acids on the adsorption of Cd^{2+} and Pb^{2+} by goethite

and montmorillonite. To our knowledge, however, no study has been done to experiment and model the adsorption of metals onto smectite in the presence of carboxylic acids.

Both sorption and precipitation are believed to be significant mechanisms for the immobilization of metals and the subsequent low leachate concentrations. The electrostatically bound cations (interlayer cations) can undergo exchange with the cations in solution in reactions which are fast, stoichiometric and reversible [15-17]. The cation exchange reaction of a metal B (Pb or Zn), of valency Z_B (2 in this study), exchanging with a cation A (Na or Ca), of valency Z_A (1 or 2, respectively), in the interlayer of a clay mineral (here the montmorillonite SWy2) can be expressed as:



Sorption by cation exchange is characterised by a strong dependency on background electrolyte concentration, a weak dependency on pH and linear sorption. The second category of reactive sites is perceived as being amphoteric surface hydroxyl groups ($\equiv\text{SOH}$) situated along the edges of the clay platelets [18]. These “edge” or “broken bond” sites, consistent with a surface complexation mechanism, exhibit a strong pH dependence and a weak dependence on ionic strength. As they can protonate and deprotonate, the concentrations of neutral ($\equiv\text{SOH}$), protonated ($\equiv\text{SOH}_2^+$) and de-protonated ($\equiv\text{SO}^-$) edge sites change as a function of pH.

The objective of this work is to reproduce the chemical conditions of an acidic leachate in a young subsurface waste landfill (pH = 5) and to understand and model the mechanisms of interaction between metallic pollutants (Pb, Zn) and smectite with a fixed ionic strength and in the presence of organic molecules such as acetic acid/acetate.

2. Materials and methods

2.1. Clay material

The clay materials used in this study were prepared from SWy2 montmorillonite, supplied by the Source Clays Repository of The Clay Minerals Society (<http://www.clays.org/SOURCE/CLAYS/SCSCavailable.html>), with the following procedure. In each Nalgene centrifuge tube, 2 g of SWy2 and 50 mL of a 1M NaCl solution were mixed on a SRT1 Stuart Scientific roller mixer for 24h, and the mixture was centrifuged. The supernatant chloride solution was then discarded and the tube was refilled with 50 mL of 1M NaCl solution. This exchange procedure was repeated five times. The sample was then introduced into dialysis membrane tubing and placed in deionised water to remove excess sodium and chloride. The water was changed daily until chloride was not detected by an AgNO₃ precipitation test. This Na-saturated clay sample was dispersed in deionized water and the fine fraction (< 2 μm) isolated by sedimentation, by applying Stokes' law. The < 2 μm Na-saturated clay fraction was dried and finely hand ground in an agate mortar. This clay sample is hereafter named Na-SWy2. Part of the Na-SWy2 stock was saturated with Ca using the same procedure as above but with a 1M CaCl₂ solution instead of NaCl. This sample is hereafter named Ca-SWy2. The BET specific surface area is 45.4 m² g⁻¹ for Na-SWy2 [19] and 46 m² g⁻¹ for Ca-SWy2. Cation exchange capacity (CEC) determined using the triethylenetetramino copper II complex method [20] is 0.850 ± 0.027 mol/kg for Na-SWy2 [19] and 0.851 ± 0.001 mol/kg for Ca-SWy2.

2.2. Solutions preparation

All solutions were prepared from analytical grade products with Millipore Milli-Q 18 MΩ water. Pb and Zn stock solutions were prepared from Pb(NO₃)₂ (Prolabo R.P. Normapur) and

Zn(NO₃)₂·6H₂O (Prolabo Rectapur) salts, respectively. The initial concentrations of Pb(NO₃)₂ and Zn(NO₃)₂ ranged from 10⁻⁶ to 10⁻² M in these stock solutions. 0.04 M NaCl and 0.02 M CaCl₂ background electrolyte solutions were prepared at pH 5 using an acetic acid/acetate pH buffer (pK_a = 4.76) at two different concentrations (0.01 M CH₃COOH and 0.03 M CH₃COONa, or 0.001 M CH₃COOH and 0.003 M CH₃COONa, respectively named high and low concentrations).

2.3. Batch sorption experiments

200 mg of Na-SWy2 or Ca-Swy2 samples were pre-equilibrated with 19.5 mL aliquots of the pH buffered NaCl and CaCl₂ stock solutions in centrifuge tubes. The tubes were rotated on a SRT1 Stuart Scientific roller mixer for 16 hours. 0.5 mL of Zn or Pb stock solutions were then added to reach a solid to liquid ratio ($r_{S/L}$) of 10 g L⁻¹. After 16 hours, the tubes were centrifuged at a relative centrifugal field of 4500 g for 15 min. Supernatant solutions were filtered through a Millipore filter (0.2 μm nitrocellulose membrane) and analyzed by atomic absorption spectrometry (AAS) using a Hitachi Z-8100 spectrophotometer. A flame spectrometer was used to measure Pb concentrations ranging from 5x10⁻⁶ to 10⁻³ M and Zn concentrations ranging from 1.5x10⁻⁶ to 6x10⁻⁵ M. A graphite atomizer enabled the measurements of Pb concentrations from 7x10⁻⁸ to 4x10⁻⁶ M. From measurements of the pollutant concentration in solution before and after interaction with smectite, the amount of metal adsorbed on the clay was quantified. Concentrations of sorbed Zn and Pb onto clay ([Zn]_{sorbed} and [Pb]_{sorbed} in mol kg⁻¹) were calculated according to:

$$[Zn]_{sorbed} = \frac{[Zn]_{tot} - [Zn]_{eq}}{r_{S/L}}$$

$$[Pb]_{sorbed} = \frac{[Pb]_{tot} - [Pb]_{eq}}{r_{S/L}}$$

where $[i]_{tot}$ stands for the total concentration of metal i measured in the initial solution and $[i]_{eq}$ stands for the concentration at equilibrium.

Error bands were calculated according to Danzer [21]. The extended combined uncertainty $U([i])$ represents an interval that contains a large part of the values of series of measurements:

$$U([i]) = k \times u([i])$$

where the selected coverage factor k was 2, to cover an interval in which 95.5% of the values are found.

Where $u([i]_{eq}) = 2\% [i]_{eq}$; $u([i]_{tot}) = 2\% [i]_{tot}$

$$\text{And } u([i]_{sorbed}) = \sqrt{(u([i]_{eq})^2 + u([i]_{tot})^2)}$$

Since the results are presented as $\log [i]_{sorbed}$ versus $\log [i]_{eq}$, the error bands become:

$$U^+ = \log ([i] + 2 u([i])) - \log([i])$$

$$U^- = \log ([i] - 2 u([i])) - \log([i])$$

2.4. Infrared spectroscopy

Fourier-transform infrared (FTIR) spectra were recorded in transmission mode using a NICOLET Magna-IR 760 Fourier transform spectrometer and a NICOLET Nic-Plan microscope. The powder sample was directly deposited on the NaCl window of the microscope stage without further preparation to avoid K^+ -clay cation exchange within the sample during analysis [22] and to prohibit contributing absorbed water from KBr pellets in the stretching O-H range. Prior to and during measurement, the spectrometer and microscope chambers were purged with dry compressed air to remove most of the atmospheric H_2O and CO_2 . The sample area analysed was a 100 μm diameter circle selected under the microscope 15 X Cassegrainian objective. Operating conditions were 128 scans with 2 cm^{-1} resolution

without CO₂-H₂O corrections. The studied wave number ranged from 650 to 4000 cm⁻¹ according to the spectrometer beamsplitter and the microscope detector (Nicolet MCT-A).

2.5. Modelling

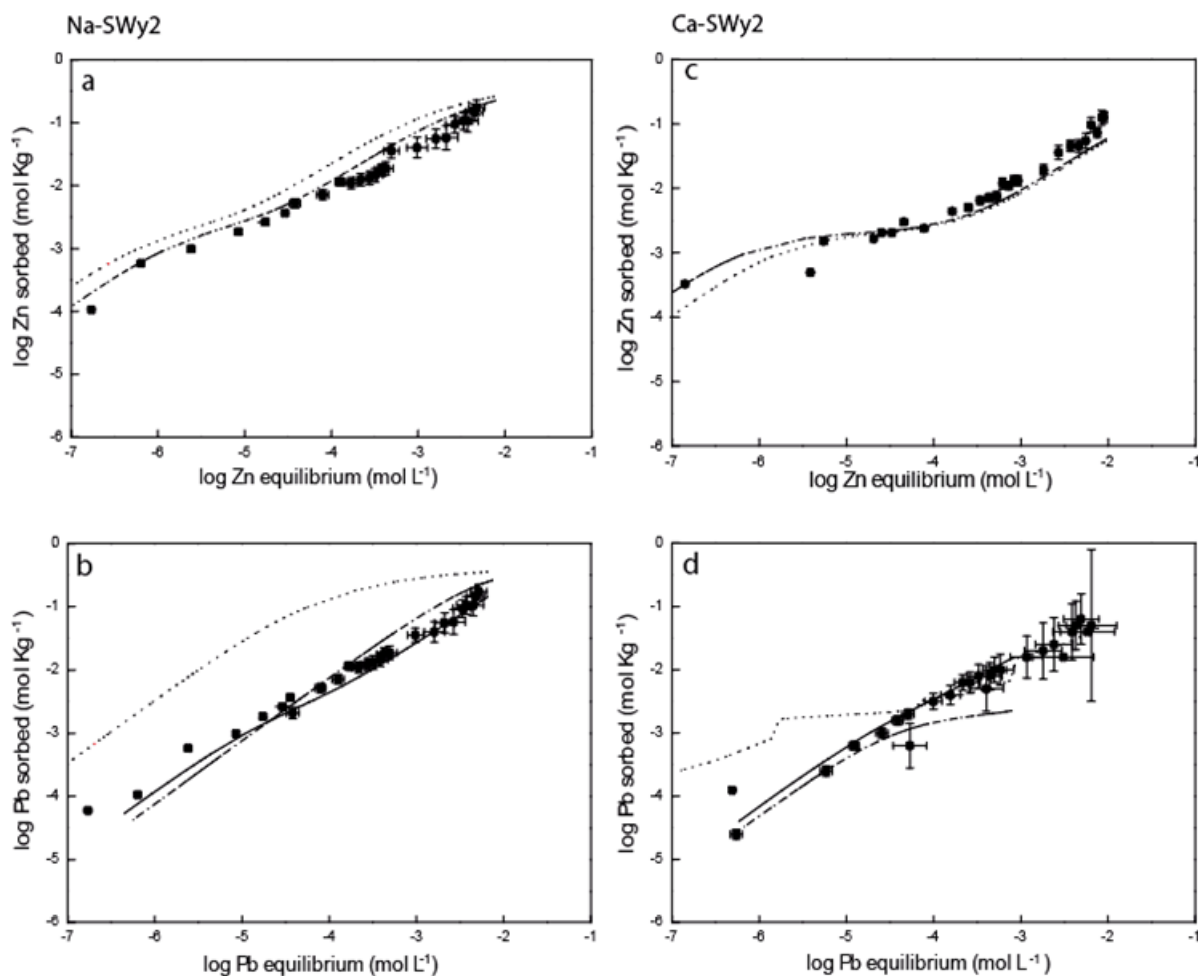
Various thermodynamic sorption models based on cation exchange and/or surface complexation mechanisms have been developed [23-27]. Bradbury and Baeyens [23] chose the diffuse double layer (DDL) model described by Stumm and Morgan [28] to develop the two site protolysis model with no electrostatic term (2SPNE model). This empirical 2SPNE model, developed by fitting titration and metal sorption data on Na-montmorillonite, was used in this study. The total ≡SOH site capacity for Na-montmorillonite, determined by titration experiments [29], is 0.08 mol sites kg⁻¹. The non-linearity of the sorption processes indicated that at least two types of sites with different affinities are involved in the overall sorption on Na-montmorillonite [23]. The so-called "strong" sites (≡S^SOH) have a low capacity and a high sorption affinity, whereas the "weak" sites (≡S^WOH) have a considerably larger capacity but a much lower sorption affinity. From the 2SPNE modelling of the titration results, Bradbury and Baeyens [23] deduced fixed values for ≡S^SOH and ≡S^WOH site capacities and protolysis constants, which are reported in Table 2. The geochemical PHREEQC2 code [30] was used in all of the fitting/modelling work described further in this study. The PHREEQC2 thermodynamic database was used throughout. The approach was to model the sorption of lead or zinc on the Na- or Ca-SWy2 clay in the same conditions as in batch experiments. For this, the CEC value measured for Na- and Ca-SWy2 was incorporated in the code, as well as the background electrolyte concentration, the concentration of the initial metal solution, the fixed solid/liquid ratio and the fixed pH value. Selectivity coefficients for Zn-Na and Zn-Ca exchange reactions (Table 3), determined by Bradbury and Baeyens [23,31], were included in

the code to model cation exchange and surface complexation reactions of zinc with Na- and Ca-montmorillonites. In contrast to zinc, only few thermodynamic data are available for lead in the literature. The procedure adopted here was to model Pb adsorption isotherms by using Zn thermodynamic coefficients and then to find the best fit which reproduced our experimental data. The objective was to determine new thermodynamic data for Pb sorption onto montmorillonite after validating the model.

3. Results

3.1. Influence of ionic background and metal concentration on the adsorption of metals onto montmorillonite

The experimental results at fixed ionic strength ($I = 0.04 \text{ M}$) and high buffer concentration ($0.01 \text{ M CH}_3\text{COOH}$ and $0.03 \text{ M CH}_3\text{COONa}$) show that the sorbed metal concentration increases with the increase in the equilibrium metal concentration (Fig. 1).

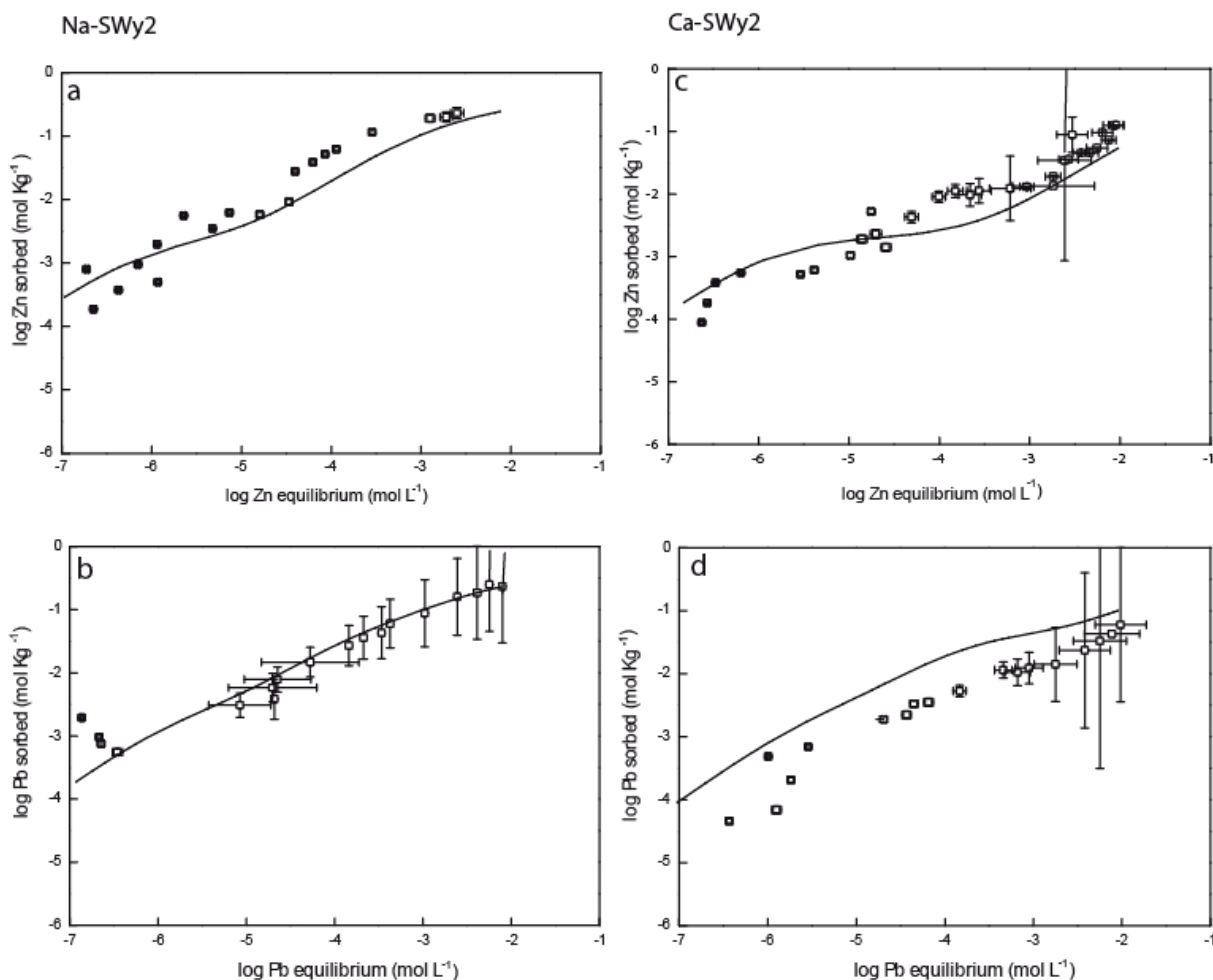


The sorption of zinc on Na-SWy2 was better than Ca-SWy2, for an equilibrium concentration between 10^{-5} and 10^{-2} M (Fig. 1a and 1c). The same results were obtained for lead (Fig. 1b and 1d). These results are in agreement with Bradbury and Baeyens [32] who determined for Eu sorption a weaker intrinsic surface complexation constant in the case of Ca-montmorillonite compared to the Na-clay and confirmed that the same trend was also true for Zn. Indeed, the binding constants of the Na-montmorillonite system are greater than those of Ca-montmorillonite. Alvarez-Ayuso and Garcia-Sanchez [33] also highlighted a lower sorption capacity of Ca-bentonite than Na-bentonite for all the metal cations studied (Cd^{2+} , Cr^{3+} , Cu^{2+} , Ni^{2+} , Zn^{2+}), which seems related to the higher charge of Ca^{2+} and its lower H^+ adsorption capacity. The replacement of low-charge (e.g. Na^+) by high-charge (e.g. Zn^{2+}) cations is favored relative to the exchange of same-charge cations (e.g. Ca^{2+} by Zn^{2+}).

The comparison of metal adsorption onto the same clay shows that lead is slightly less adsorbed than zinc onto Na-SWy2. Although Pb^{2+} has the same valence as Zn^{2+} , this cation is characterised by a larger ionic radius so its introduction in interlayers and complexation with surface sites is limited by steric hindrance and lower electrostatic attraction [7]. On the contrary, Stefan et al. [34] found a greater affinity of Pb^{2+} compared to Zn^{2+} for Na-montmorillonite. For Ca-SWy2 the difference between lead and zinc is not significant, since the same amounts of Pb and Zn were adsorbed on this smectite. This result is in agreement with Helios Rybicka et al. [11] and Auboiroux et al. [10] who showed that for trace metal concentrations, no significant difference could be discerned between lead and zinc fixation.

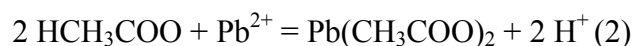
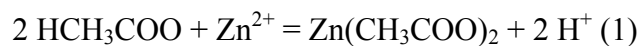
3.2. Influence of acetic acid/acetate concentration on the adsorption of metals onto montmorillonite

The adsorption of zinc and lead onto smectite in the presence of acetic acid/acetate was evaluated. For this, batch experiments were performed under the same conditions by changing only the buffer concentration. A low buffer concentration was then fixed ten times lower (0.001 M CH_3COOH , 0.003 M CH_3COONa) than the high buffer concentration (Table 1). Both for zinc and for lead, metal adsorption on Na-SWy2 significantly increased with the decrease in acetic acid/acetate concentration (Fig. 1 and 2).



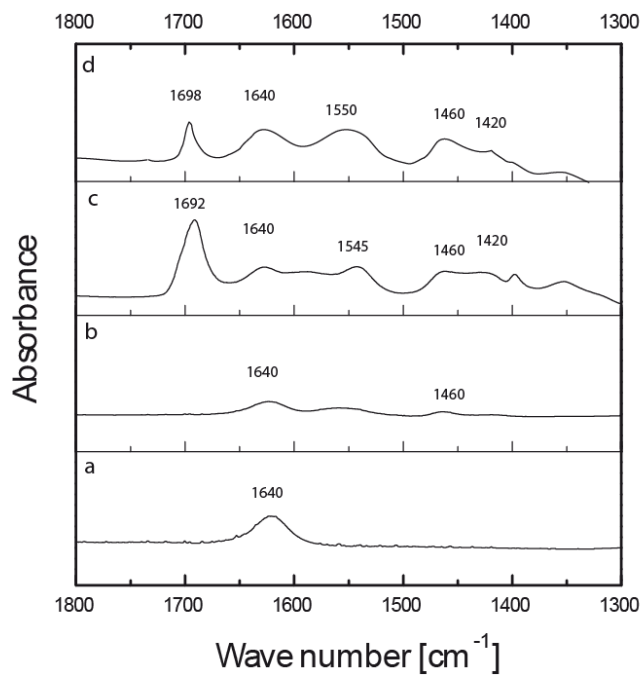
This difference was more pronounced for Zn with a higher adsorption by a logarithmic unit in the case of low buffer concentrations (Fig. 1a and 2a). Baeyens and Bradbury [29] asserted that the presence of acetic acid/acetate had no influence on the sorption of Ni and Zn on Na-montmorillonite, but this was demonstrated only in the case of low buffer concentration (0.001 M). The same trend was observed for Pb sorption onto Na-SWy2 (Fig. 1b and 2b), where the difference was more significant for low equilibrium Pb concentrations ($<10^{-6}$ M). The influence of acetic acid/acetate concentration of Zn and Pb adsorption onto Ca-SWy2 was less pronounced than onto Na-SWy2 (Fig. 1c-d and 2 c-d). Huang et al. [14] confirmed that an increase in acetic acid concentration in solution leads to a decrease in Pb^{2+} adsorption by goethite and Ca-montmorillonite. At low acid concentrations, the organic anions adsorb onto the mineral particles so that the negative surface charges increase. This weakens the ability of the acetic acid molecules to complex with Pb^{2+} ions in solution and promotes the adsorption

of Pb^{2+} . At high acetic acid concentrations, however, the concentration of Pb or Zn remaining in solution increased with increasing acid concentration and promoted the complexation of Zn^{2+} or Pb^{2+} by acid and reduced the quantity of metal ion adsorbed:



3.3. FTIR results

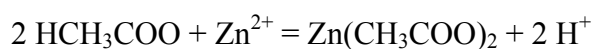
A sample of Ca-SWy2 clay powder was analyzed under the microscope to obtain the clay spectrum as reference (Fig. 3a). The band at 1640 cm^{-1} was identified as water vibration. With the addition of the buffer, peaks appeared at 1552 , 1460 and 1420 cm^{-1} (Fig. 3b). The 1420 and 1552 cm^{-1} peaks correspond respectively to symmetric and anti-symmetric stretching of $[\text{COO}]^-$ species, characteristic of acetate. The band at 1460 cm^{-1} represents asymmetric CH_3 bending modes of acetate. When zinc (10^{-4} M) was added to the system, another band appeared near 1700 cm^{-1} in addition to those described above (Fig. 3c). The same results were observed for lead onto Ca-SWy2 (Fig. 3d), and also for Zn and Pb onto Na-SWy2 (data not presented). This band is attributed to the stretching of the HO-C=O bond [35], which reveals the adsorption of acetic acid onto the clay, instead of the metals.



4. Modelling and discussion

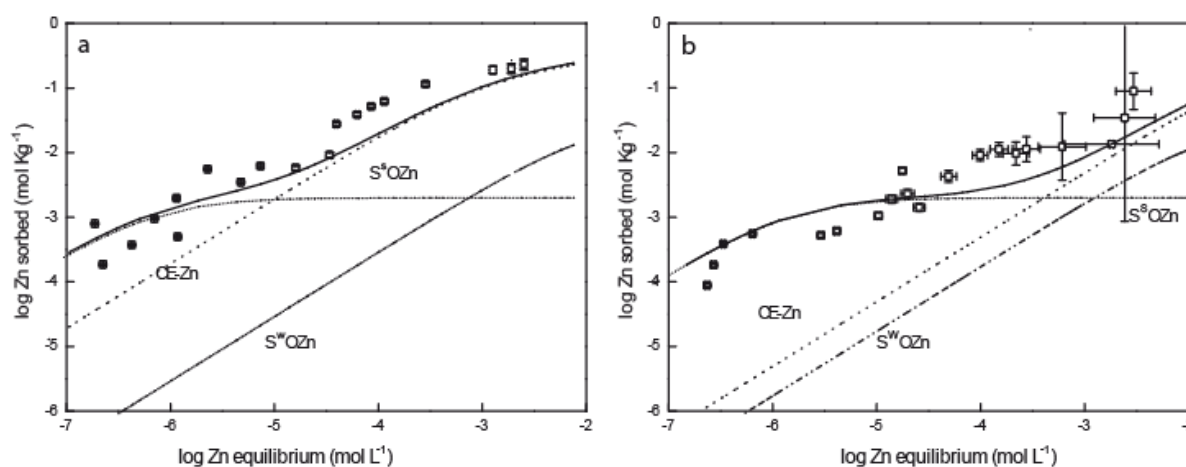
4.1. Modelling Zn sorption onto montmorillonite surfaces

Since all the parameters describing Zn sorption on conditioned Na-montmorillonite are fixed (Tables 2 and 3), the first test for the model was to compare the Zn sorption isotherm calculated at pH = 5 with the experimental measurements (Fig. 1a). The modeled curve reproduces the general trend of the experimental data well but could be improved. As previously shown by infrared spectroscopy, the acetic acid/acetate concentrations have a significant effect on the adsorption of zinc onto the clay. The equation of Zn acetate formation was therefore added in the model, as well as its thermodynamic constant (PHREEQC2 database)



With $\log K_c(\text{Zn} - \text{acetate}) = -6.5$

Fig. 1a clearly shows that the overall agreement between calculated and measured data is better in the new simulation, which validates the model. The thermodynamic data of this simulation were applied to simulate the adsorption of zinc in Na-SWy2 with a low buffer concentration; the result is shown with the continuous line in Fig. 2a. This simulation reflects, once again, the experimental data, thus confirming the model. Consequently, the mechanisms of zinc adsorption on clay can be understood as a function of Zn concentration in solution (Fig. 4a).

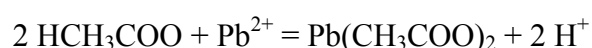


For low equilibrium zinc concentration, 90% of adsorbed zinc is fixed by surface complexation in the strong sites $\equiv\text{S}^{\text{S}}\text{OH}$. The remaining 10 % is adsorbed by cation exchange, while the influence of the weak sites is negligible. From 10^{-6} M of Zn_{eq} , adsorption by cationic exchange increases rapidly while the surface complexation onto the strong sites $\equiv\text{S}^{\text{S}}\text{OH}$ decreases. For high equilibrium zinc concentration ($> 10^{-4}$ M), all the zinc is retained in smectite by cation exchange. The same approach was adopted to model the Zn sorption data on Ca-SWy2. The first test was done by choosing the selectivity coefficient for Zn-Ca exchange in Ca-montmorillonite, $\log K_c(\text{Zn-Ca}) = 0$, as previously determined by Bradbury and Baeyens [31] (Table 3). The modeled curve exhibits the same shape as the experimental data but slightly shifted downward in the range of high Zn concentrations (Fig. 1c). The addition of the effect of Zn-acetate formation leads to a better fit of the experimental data in

the range of low Zn equilibrium concentrations. Modeling the mechanisms of zinc adsorption on Ca-SWy2 shows the same trends as for Na-SWy2 (Fig. 4b). Surface complexation by the strong sites $\equiv\text{S}^{\text{S}}\text{OH}$ is the main mechanism involved for low equilibrium zinc concentration, whereas zinc is mostly retained by cation exchange beyond 10^{-4} M. It is noticeable that around 10% of zinc is adsorbed in the weak sites $\equiv\text{S}^{\text{W}}\text{OH}$ in the case of 10^{-2} M $[\text{Zn}_{\text{eq}}]$, and the contribution of the strong sites $\equiv\text{S}^{\text{S}}\text{OH}$ is almost negligible due to their saturation.

4.2. Modelling Pb sorption onto montmorillonite surfaces

Unlike zinc, thermodynamic data of lead adsorption onto clays are sparse in the literature. The approach was as follows: first, the thermodynamic parameter of zinc for Na-SWy (log $K_c = 0.59$) [23] was introduced in the model, and the first simulation was compared to the experimental data of lead adsorption on Na-SWy2 (Fig. 1b, dotted line). The overall shape of the curve was incorrectly predicted. The second step was, as in the other simulations, to add the effect of lead acetate in the model:

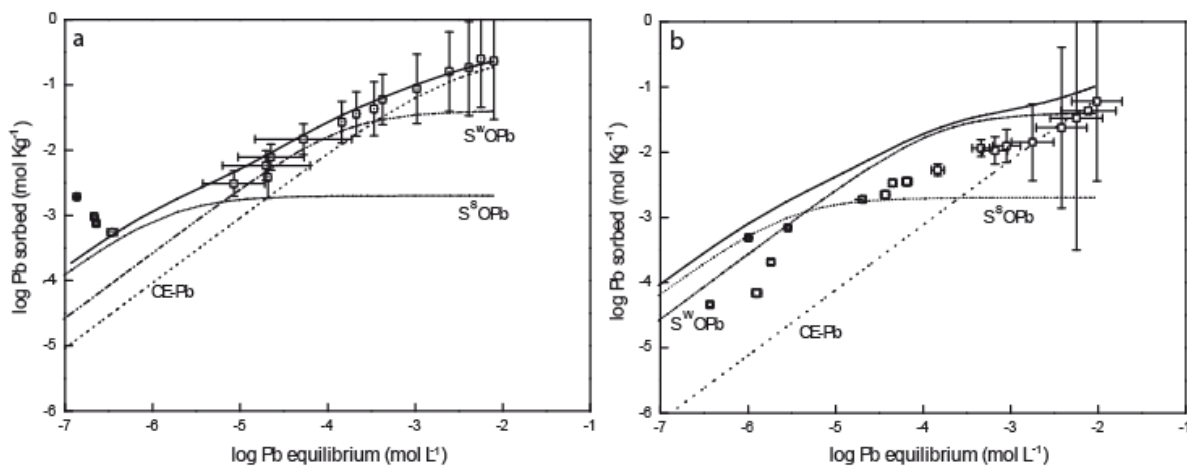


With log $K_c(\text{Pb} - \text{acetate}) = -5.5$ (PHREEQC2 database)

This second simulation is shifted downward compared to the first, indicating that part of the lead is complexed with acetate in solution (Fig. 1b, dash dotted line). While it better reproduces the shape of the experimental data, this result remains unsatisfactory, meaning that the thermodynamic data cannot be the same for zinc and lead. This was followed by an optimization procedure in which the selectivity coefficient of Pb to Na in Na-SWy2, $K_c(\text{Pb}-\text{Na})$, was varied to yield the best fit to the experimental data (Fig. 1b, continuous line). A good correspondence between calculated and measured values was obtained for log $K_c(\text{Pb}-\text{Na}) = 0.5$ (Table 3). This value was used to model the lead adsorption experiment with a low

buffer concentration in Fig. 2b. The fit corresponds very well with experimental data. Ferrell et al. [36] applied a geochemical transport model to predict lead retention by clay liners, but they only considered cationic exchange and not complexation mechanisms in the edges. Moreover, to model the cation exchange between Pb and clay, they used the database of PHREEQC2 with $\log K_c$ equal to 1.05, without experimental data to confirm this selectivity constant.

The calculated sorption isotherm of Pb on Na-SWy2 can exhibit three distinct regions depending on the Pb equilibrium concentration (Fig. 5a).

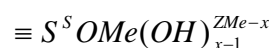


At low Pb equilibrium concentrations ($< 5 \times 10^{-6}$ M), sorption occurs mainly on the strong sites, with a maximum of 80% of Pb retained in the $\equiv S^S OH$ sites for $[Pb_{eq}] = 10^{-7}$ M. From $[Pb_{eq}] = 5 \times 10^{-6}$ M, the strong sites are saturated, so the retention of lead on the weak sites and by cation exchange increases. Pb adsorption in the $\equiv S^W OH$ sites reaches a maximum of 60% of the total adsorbed amount for $[Pb_{eq}] = 10^{-4}$ M then decreases rapidly. The contribution of Pb uptake by cation exchange is dominant for the highest Pb equilibrium concentrations ($> 10^{-3}$ M), with nearly 80% of lead retained by cation exchange at $[Pb_{eq}] = 10^{-2}$ M. The same approach was used to model the adsorption of lead onto Ca-SWy2. First, the model of Bradbury and Baeyens [31] was applied with $\log K_c = 0$, corresponding to Ca-SWy2 in interaction with Zn (Table 3), then the effect of acetic acid/acetate was taken into account by

adding the equation of lead acetate formation, $\log K_c(\text{Pb} - \text{acetate}) = -5.5$ (Fig. 1d, fine-dotted line and dash dotted line, respectively). Finally, the selectivity constant of lead for Ca-SWy2 was modified until the best agreement with the experimental data was achieved (Fig. 1d, continuous line). The best fit was found for $\log K_c(\text{Pb}-\text{Ca})$ equal to 0.3 (Table 3). The calculated sorption isotherm of Pb on Ca-SWy2 reveals that lead is differently adsorbed onto the calcic clay compared to the sodic one (Fig. 5b). Here the contribution of the weak sites is more visible over all the range of Pb equilibrium concentrations. For low Pb equilibrium concentrations ($< 10^{-6}$ M), 70% of lead uptake is located in the $\equiv\text{S}^{\text{S}}\text{OH}$ sites, 30% in the $\equiv\text{S}^{\text{W}}\text{OH}$ sites and cation exchange is not involved in this concentration range. From 10^{-5} M to $10^{-4.5}$ M $[\text{Pb}_{\text{eq}}]$, the contribution of strong sites decreases and conversely the adsorption by the weak sites increases for a maximum of 85% lead adsorbed by the weak sites. For $[\text{Pb}_{\text{eq}}] > 10^{-4.5}$ M, the proportion of lead adsorbed by complexation mechanisms in the edges decreases rapidly, and is replaced by the cation exchange mechanism. For the highest Pb equilibrium concentration (10^{-2} M), 60% of the adsorbed lead is retained by the Ca-Pb exchange mechanism, while the weak sites contribute 40% and adsorption by the strong sites, which are already saturated, is insignificant.

4.3. Linear free energy relationship

The general form for hydrolysed species of a metal Me with a valency Z_{Me} can be written as $\text{Me}(\text{OH})_x^{Z_{\text{Me}}-x}$ where x is an integer greater than or equal to unity. Consequently, the general form of the surface complex can be expressed as

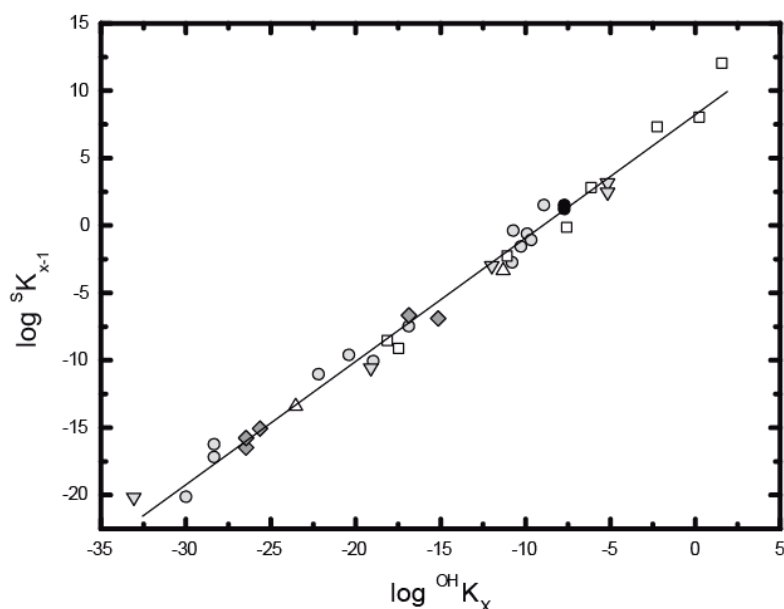


For example, for $x = 2$, the hydrolysed form of Zn is $\text{Zn}(\text{OH})_2$ and its surface complex is $\equiv\text{S}^{\text{S}}\text{OZn}(\text{OH})$. It is well established that relationships can be found between the free energies

of formation of metal complexes and thermodynamic properties of the metal ions or ligands. Such dependencies are commonly termed linear free energy relationships (LFER). Bradbury and Baeyens [37] determined a linear correlation between the logarithms of surface complexation constants of some metals adsorbed on the strong sites ($\log {}^S K_{x-1}$) of montmorillonite and their hydrolysis constants ($\log {}^{OH} K_x$):

$$\log {}^S K_{x-1} = 8.1 \pm 0.3 \pm (0.90 \pm 0.02) \log {}^{OH} K_x$$

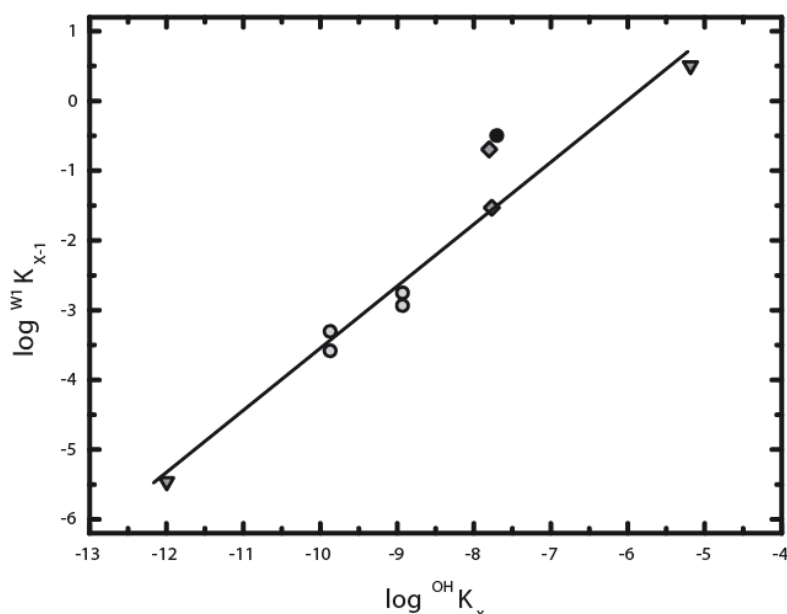
Consequently, our thermodynamic data obtained for lead adsorption onto the strong sites of Na-SWy2 and Ca-SWy2 (black circles) were plotted on Fig. 6.



They are positioned very well on this correlation line. This indicates that the chemical bonding mechanisms of metal cations with the surface hydroxyl groups of montmorillonite and aqueous hydrolysis are similar. The same approach can be applied for the weak adsorption sites. Fig. 7 shows the linear correlation between surface complexation constants of species adsorbed on the weak sites of montmorillonite exchanged with various cations and the corresponding hydrolysis constants [37]:

$$\log {}^W K_{x-1} = 6.2 \pm 0.8 \pm (0.98 \pm 0.09) \log {}^{OH} K_x$$

Similarly, the thermodynamic data obtained in this study for lead adsorption onto the weak sites of Na-SWy2 and Ca-SWy2 (black circles) were plotted on Fig. 7.



These two points established for lead are superimposed and do not fit so well with the correlation line. As explained by Bradbury and Baeyens [37], the pool of data suitable for determining weak site surface complexation constants is much smaller, and thus the confidence in the correlation in LFERs between the surface complexation constants and hydrolysis constants is not as high as in the case of the strong sites.

5. Conclusion

Zn(II) and Pb(II) adsorptions onto Na- and Ca-saturated Wyoming montmorillonites were separately investigated in acidic conditions with a fixed pH value of 5. For a given metallic cation (Zn^{2+} or Pb^{2+}), adsorption onto the sodic smectite is higher than onto the calcic one, over the whole range of metal concentrations investigated (10^{-6} to 10^{-2} M). Besides, zinc has a slightly better affinity for Na-SWy2 than lead, whereas no significant difference between the two metals was observed in the case of Ca-SWy2. The amount of metal (either zinc or lead) adsorbed onto both montmorillonites increases with the decrease in acetic acid/acetate

concentration, due to the probable formation of zinc and lead acetate complexes in solution. In addition to batch experiments, the two site protolysis model with no electrostatic term (2SPNE model) was used to fit the experimental data. In the case of zinc, the selectivity coefficients characterizing cation exchange and surface complexation reactions with Na- [23] or Ca-saturated montmorillonite [31] were incorporated in the code, as well as the thermodynamic constant of Zn-acetate formation. As the experimental data of Zn sorption were well fitted, this model was validated and used afterwards for lead. New selectivity coefficients have been determined for Pb adsorption onto Na-montmorillonite: first for cation exchange with $\log K_c(\text{Pb-Na}) = 1.5$, and then for surface complexation into the strong sites with $\log {}^S K_{\text{int}} = 1.5$, and into the weak sites with $\log {}^W K_{\text{int}} = -0.5$. Concerning the modelling of Pb(II) adsorption onto Ca-montmorillonite, the best fit was found for $\log K_c(\text{Pb-Ca})$ equal to 0.3. The surface complexation constants of Pb sorbing on the strong sites of Na- and Ca-saturated montmorillonites are well correlated with the corresponding hydrolysis constants, as Pb data verified the Linear Free Energy Relationship previously established by Bradbury and Baeyens [37].

For both Na- and Ca-saturated montmorillonites, zinc is mostly retained by cation exchange for high equilibrium zinc concentration, whereas surface complexation by the strong sites $\equiv\text{S}^{\text{S}}\text{OH}$ is the main mechanism involved below 10^{-4} M, which corresponds to zinc concentrations of the most biodegradable leachates in subsurface waste landfill. The main mechanisms involved in lead adsorption differ from Na- to Ca-saturated montmorillonites, and depend also on Pb equilibrium concentrations. In the range of the mean Pb concentrations in leachates (10^{-7} to 10^{-6} M), sorption occurs mainly on the strong sites. However, the retention of lead on the weak sites is dominant in the case of the maximum Pb concentration reported in leachates (2.4×10^{-5} M), then cation exchange takes over for the highest Pb equilibrium concentrations (10^{-2} M). This study shows that calcic montmorillonite and

especially sodic montmorillonite have a good capacity to retain zinc as well as lead, which ensures the durability of the retention performances of the clayey barriers. However, leachates of waste landfill also contain organic molecules such as acetic acid and acetate which may inhibit the adsorption of heavy metals. It should be borne in mind that the biodegradable and acidic leachates produced during the first phase of waste decomposition may contribute to the main potential risk of pollution.

Acknowledgements

The authors are grateful to Fabien Veillon for technical assistance. The two anonymous reviewers are gratefully acknowledged for their useful comments. The authors also express their gratitude to the French National Agency for Research (ANR) for the financial support. This publication is a contribution to the ANR-07-JCJC-0013-01 (Metalclay) project allocated to L. Le Forestier.

References

- [1] P. Kjeldsen, M.A. Barlaz, A.P. Rooker, A. Baun, A. Ledin, T.H. Christensen, *Crit. Rev. Environ. Sci. Technol.* 32 (2002) 297.
- [2] A. Amokrane, C. Comel, J. Véron, *Water Res.* 31 (1997) 2775.
- [3] J. Harmsen, *Water Res.* 17 (1983) 669.
- [4] P. Srivastava, B. Singh, M. Angove, *J. Colloid Interface Sci.* 290 (2005) 28.
- [5] T.H. Christensen, P. Kjeldsen, P.L. Bjerg, D.L. Jensen, J.B. Christensen, A. Baun, H.J. Albrechtsen, G. Heron, *Appl. Geochem.* 16 (2001) 659.
- [6] World Health Organization, *Guidelines for drinking-water quality, third edition incorporating the first and second addenda, Vol. 1*, Geneva, 2008.
- [7] O. Abollino, M. Aceto, M. Malandrino, C. Sarzanini, E. Mentasti, *Water Res.* 37 (2003) 1619.
- [8] S. Sen Gupta, K.G. Bhattacharyya, *Appl. Clay Sci.* 30 (2005) 199.
- [9] M.F. Brigatti, F. Corradini, G.C. Franchini, S. Mazzoni, L. Medici, L. Poppi, *Appl. Clay Sci.* 9 (1995) 383.
- [10] M. Auboiroux, P. Baillif, J.C. Touray, F. Bergaya, *Appl. Clay Sci.* 11 (1996) 117.
- [11] E. Helios Rybicka, W. Calmano, A. Breger, *Appl. Clay Sci.* 9 (1995) 369.
- [12] X. Gu, L.J. Evans, *J. Colloid Interface Sci.* 307 (2007) 317.
- [13] M. Gautier, F. Muller, J.M. Bény, L. Le Forestier, P. Albéric, P. Baillif, *Clay Miner.* 44 (2009) 207.
- [14] L. Huang, H. Hu, X. Li, L.Y. Li, *Appl. Clay Sci.* 49 (2010) 281.
- [15] G.I. Gaines, H.C. Thomas, *J. Chem. Phys.* 21 (1953) 714.
- [16] H. Van Olphen, *An introduction to clay colloid chemistry*, Interscience Publishers, New York, 1963.

- [17] G.H. Bolt, Thermodynamics of cation exchange, in: G.H. Bolt (Ed.), Soil chemistry B. Physico-chemical models, Elsevier, Amsterdam, 1982, p. 27-46.
- [18] G. Sposito, The surface chemistry of soils, Oxford University Press, New York, 1984.
- [19] L. Le Forestier, F. Muller, F. Villiéras, M. Pelletier, Appl. Clay Sci. 48 (2010) 18.
- [20] L. Ammann, F. Bergaya, G. Lagaly, Clay Miner. 40 (1995) 441.
- [21] K. Danzer, Analytical chemistry, Theoretical and metrological fundamentals, Springer, Heidelberg, 2007.
- [22] M. Pelletier, L.J. Michot, O. Barrès, B. Humbert, S. Petit, J.L. Robert, Clay Miner. 34 (1999) 439.
- [23] M.H. Bradbury, B. Baeyens, J. Contam. Hydrol. 27 (1997) 223.
- [24] B.R. Bickmore, K.M. Rosso, R.T. Nagy, R.T. Cygan, C.J. Tadanier, Clays Clay Miner. 51 (2003) 359.
- [25] C. Tournassat, E. Ferrage, C. Poinson, L. Charlet, J. Colloid Interface Sci. 273 (2004) 234.
- [26] E. Tertre, S. Castet, G. Berger, M. Loubet, E. Giffaut, Geochim. Cosmochim. Acta 70 (2006) 4579.
- [27] I.C. Bourg, G. Sposito, A.C.M. Bourg, J. Colloid Interface Sci. 312 (2007) 297.
- [28] W. Stumm, J.J. Morgan, Aquatic Chemistry, Wiley, New York, 1981.
- [29] B. Baeyens, M.H. Bradbury, J. Contam. Hydrol. 27 (1997) 199.
- [30] D.L. Parkhurst, C.A.J. Appelo, User's guide to PHREEQC (Version 2) - A computer program for speciation, batch-reaction, one-dimensional transport, and inverse geochemical calculations, Water Resources Investigations, US Geological Survey, Denver, Colorado (Report 99-4259), 1999.
- [31] M.H. Bradbury, B. Baeyens, Geochim. Cosmochim. Acta 63 (1999) 325.
- [32] M.H. Bradbury, B. Baeyens, Geochim. Cosmochim. Acta 66 (2002) 2325.

[33] E. Alvarez-Ayuso, A. Garcia-Sanchez, *Clays Clay Miner.* 51 (2003) 475.

[34] M. Stefan, D.S. Stefan, I.A. Marinescu, M. Belcu, D.I. Vaireanu, *Rev. Roum. Chim.* 53 (2008) 965.

[35] J.D. Kubicki, *Geochim. Cosmochim. Acta* 63 (1999) 2709.

[36] R.E. Ferrell, P. Aagaard, J. Forsman, L. Greenwood, Z. Zheng, *Appl. Clay Sci.* 21 (2002) 59.

[37] M.H. Bradbury, B. Baeyens, *Geochim. Cosmochim. Acta* 69 (2005) 875.

Figure captions

Fig. 1

Metal adsorption isotherms onto montmorillonite at pH = 5, fixed ionic strength ($I = 0.04 \text{ M}$) and high buffer concentration ($0.01 \text{ M CH}_3\text{COOH}$ and $0.03 \text{ M CH}_3\text{COONa}$). $r_{SL} = 10 \text{ g L}^{-1}$.

■: experimental data. Fig. 1a and 1b: the dotted line is obtained using the Bradbury and Baeyens model [23] with the fixed parameters: $\log K_c(\text{Zn-Na}) = 0.59$, $\log {}^S K_{\text{int}}(\text{Zn}) = 1.6$ and $\log {}^W K_{\text{int}}(\text{Zn}) = -2.7$. Fig. 1c and 1d: the dotted line is obtained using the Bradbury and Baeyens model [31] with the fixed parameters: $\log K_c(\text{Zn-Ca}) = 0$, $\log {}^S K_{\text{int}}(\text{Zn}) = 1.2$ and $\log {}^W K_{\text{int}}(\text{Zn}) = -2.9$. Fig. 1a-b-c-d: the dash dotted lines are obtained by using the same model and by adding the potential formation of Zn acetate ($\log K_c(\text{Zn - acetate}) = -6.5$) or Pb acetate ($\log K_c(\text{Pb - acetate}) = -5.5$), with no fitted parameters. Fig. 1b: the continuous line is the best fit to the data, with the following fit parameters: $\log K_c(\text{Pb-Na}) = 0.50$, $\log {}^S K_{\text{int}}(\text{Pb}) = 1.5$ and $\log {}^W K_{\text{int}}(\text{Pb}) = -0.5$. Fig. 1d: the continuous line is the best fit to the data, with the following fit parameters: $\log K_c(\text{Pb-Ca}) = 0.30$, $\log {}^S K_{\text{int}}(\text{Pb}) = 1.2$ and $\log {}^W K_{\text{int}}(\text{Pb}) = -0.5$.

Fig. 2

Metal adsorption isotherms onto montmorillonite at pH = 5, fixed ionic strength ($I = 0.04 \text{ M}$) and low buffer concentration ($0.001 \text{ M CH}_3\text{COOH}$ and $0.003 \text{ M CH}_3\text{COONa}$). $r_{SL} = 10 \text{ g L}^{-1}$.

□: experimental data. The continuous lines correspond to the fit with the selectivity coefficients for Zn-Na and Pb-Na equilibria on Na-SWy2, and Zn-Ca and Pb-Ca equilibria on Ca-SWy2 (Table 3).

Fig. 3

FTIR spectra of Ca-SWy2 in interaction with different solutions. (a) Ca-SWy2 in powder used as reference, (b) Ca-SWy2 in interaction with buffer solution at high concentration (0.01 M CH₃COOH and 0.03 M CH₃COONa), (c) Ca-SWy2 in interaction with buffer solution at high concentration and Zn(NO₃)₂ at 10⁻⁴ M, (d) Ca-SWy2 in interaction with buffer solution at high concentration and Pb(NO₃)₂ at 10⁻⁴ M

Fig. 4

Zn sorption isotherm and contribution of the different surface species for Zn sorption onto Na-SWy2 and Ca-SWy2 at pH = 5 in 0.04 M NaCl or 0.02 M CaCl₂, respectively, and with low buffer concentration (0.001 M CH₃COOH and 0.003 M CH₃COONa). $r_{SL} = 10 \text{ g L}^{-1}$. (a) Zn sorption onto Na-SWy2. □: experimental data. The continuous line is calculated using the Bradbury and Baeyens model [23] with the fixed parameters ($\log K_c(\text{Zn-Na}) = 0.59$, $\log {}^S K_{\text{int}}(\text{Zn}) = 1.6$ and $\log {}^W K_{\text{int}}(\text{Zn}) = -2.7$), and by adding the potential formation of Zn acetate ($\log K_c(\text{Zn - acetate}) = -6.5$). Dotted line: cation exchange (CE-Zn); fine-dotted line: complexation in the strong sites ($\equiv \text{S}^{\text{S}}\text{OZn}^+$); dash dotted line: complexation in the weak sites ($\equiv \text{S}^{\text{W}}\text{OZn}^+$). (b) Zn sorption isotherm onto Ca-SWy2. □: experimental data. The continuous line is calculated using the Bradbury and Baeyens model [31] with the fixed parameters ($\log K_c(\text{Zn-Ca}) = 0.$, $\log {}^S K_{\text{int}}(\text{Zn}) = 1.2$ and $\log {}^W K_{\text{int}}(\text{Zn}) = -2.9$), and by adding the potential formation of Zn acetate ($\log K_c(\text{Zn - acetate}) = -6.5$). Dotted line: cation exchange (CE-Zn); fine-dotted line: complexation in the strong sites ($\equiv \text{S}^{\text{S}}\text{OZn}^+$); dash dotted line: complexation in the weak sites ($\equiv \text{S}^{\text{W}}\text{OZn}^+$).

Fig. 5

Pb sorption isotherm and contribution of the different surface species for Pb sorption onto Na-SWy2 and Ca-SWy2 at pH = 5 in 0.04 M NaCl or 0.02 M CaCl₂, respectively, and low buffer

concentration (0.001 M CH₃COOH and 0.003 M CH₃COONa). $r_{SL} = 10 \text{ g L}^{-1}$. (a) Pb sorption isotherm onto Na-SWy2. □: experimental data. The continuous line is the best fit to the data obtained by using the Bradbury and Baeyens model [23] and the contribution of Pb acetate ($\log K_c(\text{Pb} - \text{acetate}) = -5.5$). Fit parameters: $\log K_c(\text{Pb-Na}) = 0.5$, $\log {}^S K_{\text{int}}(\text{Pb}) = 1.5$ and $\log {}^W K_{\text{int}}(\text{Pb}) = -0.5$. Dotted line: cation exchange (CE-Pb); fine-dotted line: complexation in the strong sites ($\equiv \text{S}^{\text{S}}\text{OPb}^+$); dash dotted line: complexation in the weak sites ($\equiv \text{S}^{\text{W}}\text{OPb}^+$). (b) Pb sorption isotherm onto Ca-SWy2. □: experimental data. The continuous line is the best fit to the data obtained by using the Bradbury and Baeyens model [31] and the contribution of Pb acetate ($\log K_c(\text{Pb} - \text{acetate}) = -5.5$). Fit parameters: $\log K_c(\text{Pb-Ca}) = 0.3$, $\log {}^S K_{\text{int}}(\text{Pb}) = 1.2$ and $\log {}^W K_{\text{int}}(\text{Pb}) = -0.5$. Dotted line: cation exchange (CE-Pb); fine-dotted line: complexation in the strong sites ($\equiv \text{S}^{\text{S}}\text{OPb}^+$); dash dotted line: complexation in the weak sites ($\equiv \text{S}^{\text{W}}\text{OPb}^+$).

Fig. 6

Correlation of surface complexation constants of species sorbing on the strong sites of montmorillonite with the corresponding hydrolysis constants. Gray circles: Mn(II), Co(II), Cd(II), Ni(II), Zn(II); gray diamonds: Eu(III), Am(III); gray squares: (Sn(IV), Th(IV)); light gray triangles: Np(V); gray inverted triangles: U(VI) (from Bradbury and Baeyens [37]). Black circles: Pb(II) on Na-SWy2 and on Ca-SWy2 (this study).

Fig. 7

Correlation of surface complexation constants of species sorbing on the weak sites of montmorillonite with the corresponding hydrolysis constants. Gray circles: Ni(II), Zn(II); gray diamonds: Eu(III); and gray inverted triangles: U(VI) (from Bradbury and Baeyens [37]). Black circles: Pb(II) on Na-SWy2 and on Ca-SWy2 (this study).

Table 1

Experimental conditions for sorption and FTIR experiments

	Clay	Salt solutions	Buffer (pH=5)		Metallic pollutants
			High concentration	Low concentration	
Batch experiments	Na-SWy2	0.04 M NaCl	0.01 M CH ₃ COOH	0.001 M CH ₃ COOH	10 ⁻⁶ - 10 ⁻² M Zn(NO ₃) ₂ and Pb(NO ₃) ₂
	Ca-SWy2	0.02 M CaCl ₂	0.03 M CH ₃ COONa	0.003 M CH ₃ COONa	
FTIR systems	a Ca-SWy2	-	-	-	-
	b Ca-SWy2	0.02 M CaCl ₂	+	-	-
	c Ca-SWy2	+	+	-	Zn(NO ₃) ₂ 10 ⁻⁴ M
	d Ca-SWy2	+	+	-	Pb(NO ₃) ₂ 10 ⁻⁴ M

Table 2

Summary of site types, site capacities, and protolysis constants on Na-SWy2 and Ca-SWy2, based on the Bradbury and Baeyens model [23]

Site types	Site capacities (moles kg ⁻¹)
$\equiv\text{S}^{\text{S}}\text{OH}$ (strong sites)	0.002
$\equiv\text{S}^{\text{W}}\text{OH}$ (total weak sites)	0.08
Surface complexation reaction	log K_{int}
$\equiv\text{S}^{\text{S}}\text{OH} + \text{H}^+ \leftrightarrow \equiv\text{S}^{\text{S}}\text{OH}_2^+$	4.5
$\equiv\text{S}^{\text{W}}\text{OH} + \text{H}^+ \leftrightarrow \equiv\text{S}^{\text{W}}\text{OH}_2^+$	4.5
$\equiv\text{S}^{\text{S}}\text{OH} \leftrightarrow \equiv\text{S}^{\text{S}}\text{O}^- + \text{H}^+$	-7.9
$\equiv\text{S}^{\text{W}}\text{OH} \leftrightarrow \equiv\text{S}^{\text{W}}\text{O}^- + \text{H}^+$	-7.9

Table 3

Summary of reactions (cation exchange and surface complexation) and selectivity coefficients for Zn-Na and Pb-Na equilibria on Na-SWy2, and Zn-Ca and Pb-Ca equilibria on Ca-SWy2.

	Na-SWy2	Ca-SWy2
Cation exchange	log K_c	
$2\text{Na-Clay} + \text{Zn}^{2+} \leftrightarrow \text{Zn-Clay} + 2\text{Na}^+$	0.59 ^a	
$\text{Ca-Clay} + \text{Zn}^{2+} \leftrightarrow \text{Zn-Clay} + \text{Ca}^{2+}$		0 ^b
$2\text{Na-Clay} + \text{Pb}^{2+} \leftrightarrow \text{Pb-Clay} + 2\text{Na}^+$	0.5	
$\text{Ca-Clay} + \text{Pb}^{2+} \leftrightarrow \text{Pb-Clay} + \text{Ca}^{2+}$		0.3
Surface complexation reaction	log K_{int}	
$\equiv\text{S}^{\text{S}}\text{OH} + \text{Zn}^{2+} \leftrightarrow \equiv\text{S}^{\text{S}}\text{OZn}^+ + \text{H}^+$	1.6 ^a	1.2 ^b
$\equiv\text{S}^{\text{W}}\text{OH} + \text{Zn}^{2+} \leftrightarrow \equiv\text{S}^{\text{W}}\text{OZn}^+ + \text{H}^+$	-2.7 ^a	-2.9 ^b
$\equiv\text{S}^{\text{S}}\text{OH} + \text{Pb}^{2+} \leftrightarrow \equiv\text{S}^{\text{S}}\text{OPb}^+ + \text{H}^+$	1.5	1.2
$\equiv\text{S}^{\text{W}}\text{OH} + \text{Pb}^{2+} \leftrightarrow \equiv\text{S}^{\text{W}}\text{OPb}^+ + \text{H}^+$	-0.5	-0.5

^a From Bradbury and Baeyens [23]

^b From Bradbury and Baeyens [31]